CubeSat Image Resolution Capabilities with Deployable Optics and Current Imaging Technology

James A. Champagne, Scott M. Hansen, Trent T. Newswander
Utah State University Research Foundation Space Dynamics Laboratory
1695 North Research Park Way, North Logan, Utah 84341; 435-713-3428
James.Champagne@sdl.usu.edu

Blake G. Crowther
Synopsys, Inc., Optical Solutions Group
199 S. Los Robles Ave, Suite 400, Pasadena, CA 91101; 626-795-9101
blakec@synopsys.com

ABSTRACT

Research in attitude determination and control, communications, power, and propulsion of CubeSats are making advances every year. Advancement in these areas of technology are required for CubeSats to be capable of increased resolution imagery. One aspect of CubeSats, and all other small satellites, remains constant: their limited volume. The volume ultimately limits the size of an optical payload. A brief survey of current Earth optical imaging satellites shows the importance of aperture size to obtain the spatial resolution required to achieve mission objectives. The Space Dynamics Laboratory (SDL) is researching deployable optical apertures in order to overcome the volume constraint on aperture diameter and telescope focal length. To date, SDL has demonstrated successful deployment repeatability of optical mirror segments and metering structures that are capable of supporting high-resolution imagery in the visible spectrum. The paper concludes with a conceptual CubeSat high resolution imager that incorporates deployable optics and current imaging technology.

INTRODUCTION

CubeSat technology continues to improve and more advanced missions are being planned and launched every year. A common goal among developers is to increase the capabilities of these small satellites and make them capable of collecting valuable data from Earth orbit. Production of high-resolution Earth imagery from CubeSats could prove to be highly useful to the scientific community and others. SDL is currently researching deployable optical apertures and metering structures that will enable high-resolution visible imagery from a CubeSat platform.

Optical aperture diameter is one of the most important parameters for collecting high spatial resolution and high signal-to-noise imagery. A survey of current Earth observation satellites shows the importance of optical aperture in achieving mission objectives and useful science. In the last two decades, there has been considerable interest in developing deployable optics for increased aperture on satellites[1,2,3]. There are a handful of groups that have recently published work on some form of deployable optics and structures suitable for CubeSats[4,5,6,7]. Deployable optical apertures and metering structures are key to capturing high spatial resolution imagery from a volume limited CubeSat platform.

Over the past 3 years, the Space Dynamics Laboratory has researched deployable mirrors suitable for imagery from a CubeSat platform. To date, the SDL research team has measured alignment repeatability of a multi-segmented powered primary mirror that is capable of supporting imagery into the visible spectrum. The team has also developed a deployable metering structure, which will allow longer focal length telescopes to be used on small volume satellites. This technology is currently being developed to deploy a Cassegrain secondary mirror but it could also be used for deploying long focal length refractive optical elements.

With current small satellite technology and deployable apertures, achieving near 1 m ground spatial resolution imagery in a CubeSat size form factor could be possible in the near future. The technical requirements of high-resolution imagery from a CubeSat platform have been investigated and a conceptual 2-3U CubeSat imager solution developed that gives a 1.5 m optics ground spot size from low Earth orbit.

APERTURE SURVERY

Current EO Satellites

Several remote sensing systems have been built and are flying on small satellites. A sampling of published data on the aperture and reported resolution of several such remote sensing systems can be seen in Table 1. The listed remote sensing systems have been developed within the last decade, which indicates the pace with which remote sensing systems are being developed.

Most remote sensing systems that are intended for use on small satellites use apertures of diameter greater than 300 mm. This enables the system to acquire scenes with ground resolutions between 1 and 4 m, depending on the altitude of the satellite. Thus, the market seems to have determined that satellite based imagery at a resolution of approximately 1 m is desirable.

In order to obtain imagery of this resolution, these remote sensing systems use satellites that are small but are significantly larger than a CubeSat. One entry in the table of example remote sensing systems, Dove-2[4], uses a CubeSat platform and has an aperture of 90 mm. Dove-2 operates at an altitude of 575 km, which enables it to collect imagery with a resolution of approximately 4.4 m. This is about the best resolution available from an optical system that is accommodated within the envelope of a CubeSat. A lower altitude could provide higher resolution imagery, but not at the 1 m level. It is clear that if high-resolution imagery is to be obtained from a CubeSat platform, it will have to be from an optical system using deployable elements.

Table 1:   Example small-satellite based remote sensing systems.

Satellite Name	Reported Aperture Diameter [mm]	Reported Resolution [m]	Reported Altitude [km]
NigeriaSat-2[8]	385	2.5	700
Beijing-1[8]	310	4	700
DubaiSat-2[9]	400	1	600
RazakSAT[10]	300	2.5	685
UrtheCast[11]	320	1	370
SkySat-1[11]		1	575
Dove-2[12]	90	4.4	575

High-resolution imagery from these satellites is required in order to meet the demands of mapping, water resource management, agricultural land use, population monitoring, health hazard monitoring, and disaster mitigation and management.

SDL DEPLOYABLE PETAL TELESCOPE

Deployable Telescope System

The deployable petal telescope (DPT) is a Cassegrain imaging system comprised of a deployable primary and secondary mirror. Deployment and alignment of both mirrors is passive, requiring no electrical energy. Stored spring energy supplies the forces necessary for deployment and fixed alignment. Although the current design is for a CubeSat, the team envisions it being adaptable to other small satellite form factors. Figure 1 panel a) shows the DPT prototype with deployed primary and secondary mirror with a baffle installed between. Red rays on panel b) indicate how incoming light is focused behind the primary mirror onto a focal plane array. Figure 2 shows both mirrors in the stowed state with baffle removed. A collapsible baffle is planned to be installed between the primary and secondary mirrors. Volume for a detector and supporting electronics is reserved behind the primary mirror. The laboratory prototype is designed to accept a commercial CCD camera for image quality tests. In the stowed configuration, the full telescope is able to fit within a 10 cm x 10 cm x 250 mm volume. It is estimated that the stowed telescope length can be reduced to 175 mm with custom packaging of the spring engine.
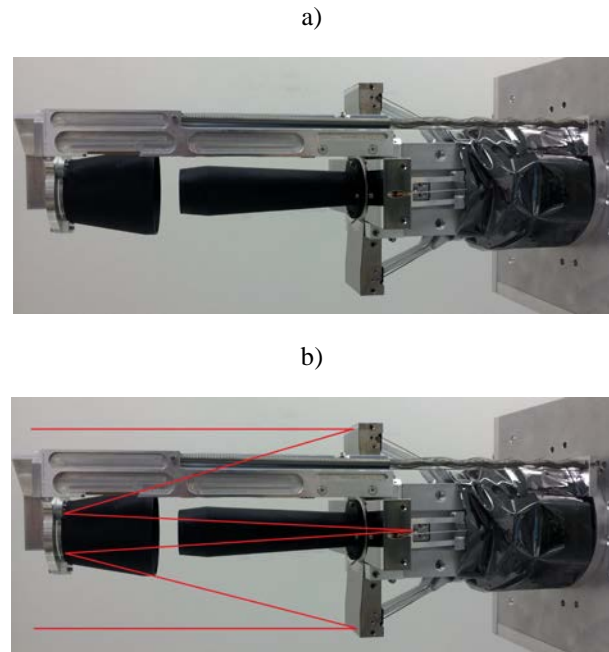
a)

b)

Figure 1: Deployable Petal Telescope Deployed in the Imaging Configuration a) without and b) with incoming rays from the left

Figure 2: Deployable Petal Telescope in the Stowed Configuration

Deployable Primary Mirror

Over the past year the DPT research team has fabricated a multi-segmented parabolic primary mirror based on the design described in "Deployable Mirror for Enhanced Imagery Suitable for Small Satellite Applications"[13]. The primary mirror is designed to have a 272 mm focal length and a powered aperture diameter of 127 mm. As a stand-alone optic, the primary mirror is fast, operating at F/1.9. Flat alignment mirrors were added at the outer edge of each mirror segment to aid in optical alignment and test, as seen in Figure 3. These features would be considerably smaller if not absent on a flight model as a large amount of optical aperture is spent on these features. Without the alignment flats, the powered aperture diameter would be 152.4 mm. The current prototype primary mirror segments are able to fold and stow within a 10 cm x 10 cm cross-section as outlined in red in Figure 4. It is estimated that the current design could be scaled up to a 200 mm aperture diameter and still fit within the same cross-section.
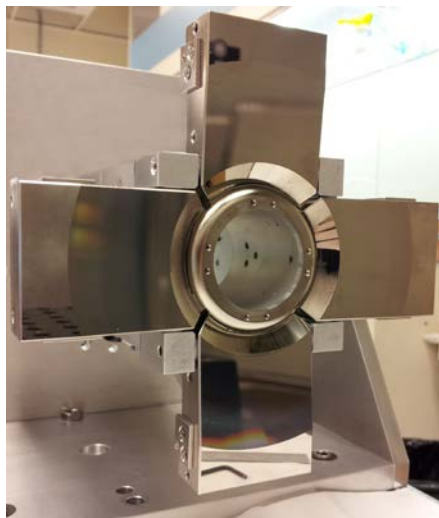

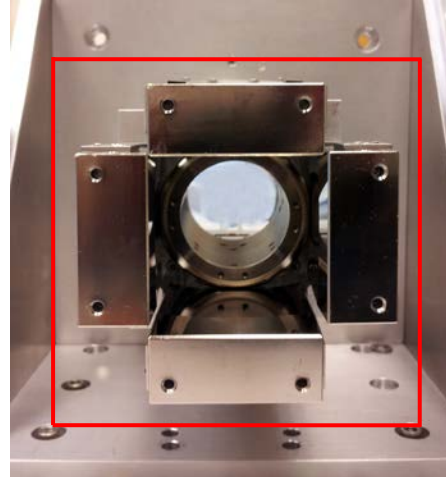**Figure 3: Deployed Primary Mirror**

Figure 4: Stowed Primary Mirror with 10 cm x 10 cm Cross-Section Outlined in Red

Fabrication and Alignment

There are many challenging aspects to aligning and operating a deployable segmented powered mirror, two of which are discussed in this paper. The first challenge is achieving best alignment of all the mirror segments relative to one another. After finishing a nearly identical optical profile on all segments, they must be aligned as close as possible in their six degrees of freedom. The three critical alignments are: piston, tip, and tilt. Figure 5 gives the coordinate system for a single petal. Piston is a highly sensitive alignment parameter and is defined as translation along the z-axis or optical axis. Tip is defined as rotation about the y-axis and tilt is rotation about the x-axis. In our case, the segments are slightly more sensitive to tilt than tip errors.
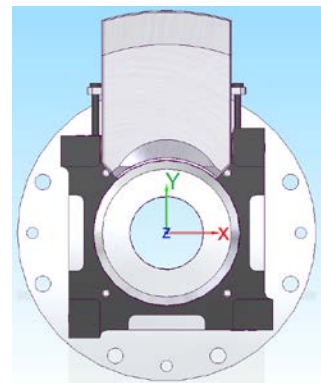

Figure 5: Mirror Coordinate System

Very precise mechanical fabrication techniques with very small error tolerances are used to align the mirror segments in piston, tip, and x-y translations. Having no adjustment mechanisms for these alignment parameters ensures they will remain stable over time. The only

adjustable alignment parameter is tilt through a supporting structure attached to the back of a mirror segment. This structural element is adjusted with the mirror in the deployed position but prior to actual operation. An interferometer is used to monitor alignment of all segments simultaneously as individual tilt alignments are adjusted.

The second challenging aspect is repeatably deploying all mirror segments back to the best alignment position. Surface deformation, friction, wear, contamination, and semi-kinematic interfaces are the limiting factors in returning the mirror segments to their best alignment.

Interferometry

A ZYGO phase shifting interferometer is used to align all four mirror segments to one another in an autocollimation null test setup as seen in Figure 6. The interferometer creates a high quality diverging spherical test wavefront that is aligned to the focal point of the primary mirror. The parabolic primary mirror collimates the wavefront after reflection which is then returned to the primary via an optical flat and re-focused by the primary back into the interferometer. Any surface or alignment errors in the primary mirror impart aberrations into the test wavefront. The test beam reflects from the primary twice in this setup, causing surface errors to be magnified by a factor of four on the wavefront. Thus the test is highly sensitive to figure and alignment errors of the individual mirror segments. The aberrated test wavefront re-enters the interferometer to interfere with the reference wavefront produced by the interferometer optics.
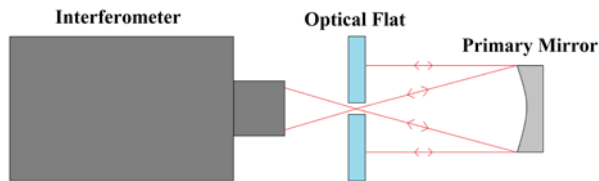

Figure 6: Autocollimation Null Test Setup

Interference between the test and reference wavefronts create a fringe pattern that shows the primary mirrors error from that of a paraboloidal surface figure. The spacing from a dark-to-dark (or bright-to-bright) fringe represents ¼ wave surface error at the HeNe illumination wavelength, or 158 nm. Figure 7 shows 8-9 tilt fringes across the aperture due to the test wavefront being tilted with respect to the reference wavefront.
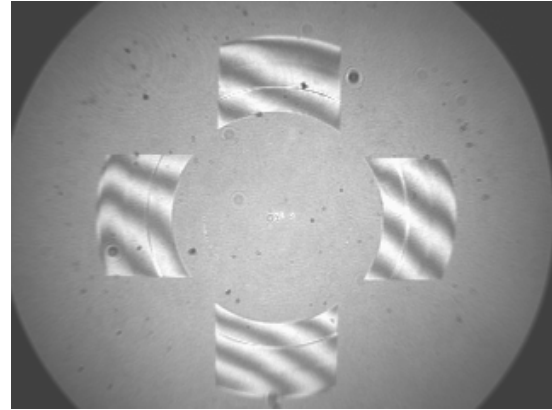

Figure 7: Deployable Primary Interferogram with Tilt Fringes

Whenever the primary's focus coincides with that of the interferometers, straight tilt fringes across the aperture indicate an excellent paraboloidal optical figure. Good mirror segment alignment is realized when the fringes are aligned to one another across the segmented apertures and have the same spatial frequency. Any deviation from straight evenly spaced fringes indicates an optical figure error. For instance, the fringes in Figure 7 show a slight curvature at the very edge of each segment. This indicates that the edge either slopes up or down approximately ½ a fringe or just under 80 nm in height. The phase shifting capability of the interferometer determines if the edge is turned up or down. In this case it is a turned down edge.

The full aperture tilt fringes can be removed by the interferometer fringe analysis software or by tilting the optical flat to obtain the null interferogram with minimum fringes across the aperture, as seen in Figure 8. The interferometer fringe analysis software is also able to subtract out any focus errors between the interferometer and primary mirror.
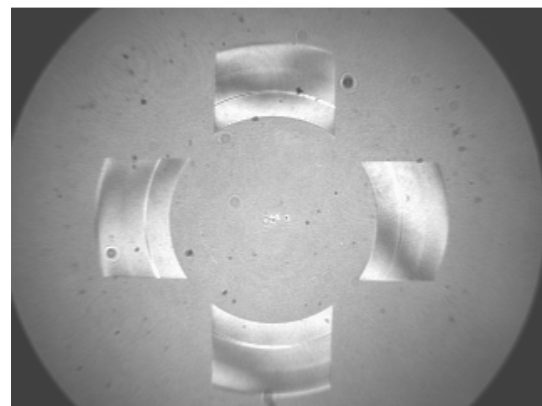

Figure 8: Deployable Primary Null Interferogram

Primary Alignment Repeatability

An alignment repeatability test was completed in order to determine repeatability errors in how well the four mirror segments passively re-align to one another. The ZYGO phase shifting interferometer was used in the autocollimation null test setup to measure the surface error of the segmented primary mirror throughout the test. Ten consecutive stow and deploy sequences were performed on the primary while aligned with the interferometer. The mean RMS surface error of the ten deployments was measured to be 25.9 nm with a two sigma standard deviation of 7.8 nm. The ten deployment statistics are listed in Table 2.

Table 2: Primary Mirror Interferometric Repeatability Statistics

Deployment #	Measured RMS Surface Error [nm]
1	25.9
2	24.7
3	22.1
4	21.5
5	23.4
6	32.9
7	22.8
8	27.0
9	27.2
10	31.6
Mean	25.9
1 σ Standard Deviation	3.9
2 σ Standard Deviation	7.8

The mean alignment error of the segments at 26 nm RMS is much greater than the 2σ repeatability error. Much of this error results from the surface error of the mirror segments rather than the positioning repeatability. The average individual mirror segment contributes 20 nm RMS to the system wavefront error. More advanced computer controlled polishing techniques such as magnetorheological finishing (MRF) or computer controlled optical surfacing (CCOS) will be able to polish the segments to better than 10 nm RMS.

Deployable Secondary

The primary mirror image quality performance of a Cassegrain telescope is typically the most critical to telescope system image quality performance. This is especially true when a small secondary mirror is mounted close to the primary requiring a fast primary with a relatively short focal length. In order to reduce the optical system sensitivity to primary mirror errors, the primary mirror F number should be as slow as possible for the application. For an F/2 primary mirror, the secondary mirror will be spaced approximately 200 mm away from the primary mirror. This will keep the secondary mirror small and provide adequate room for folding the system focal length and packaging the camera.

For the DPT, the current F/7 Cassegrain optical design requires a secondary-to-focal plane distance of 275 mm. Reserving approximately 50 mm of payload length for a focal plane array and electronics, the total camera payload length required would be 325 mm. This length can be dramatically reduced with the implementation of a deployable secondary mirror. Current estimates predict that the telescope payload length could be reduced to 175 mm, nearly a 50% reduction for this specific optical system.

It is desired to keep the secondary mirror monolithic and keep the deployment mechanism very simple. It was determined that a single non-telescoping boom located in one of the four corners outside of the primary mirror could be packaged compactly and provide the necessary structural stiffness for space operation. Figure 9 shows the secondary mirror proof of principle system attached to the primary mirror in its stowed position. Figure 10 shows the secondary mirror proof of principle system fully deployed.
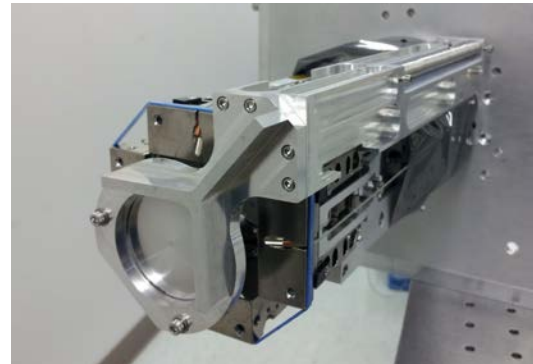

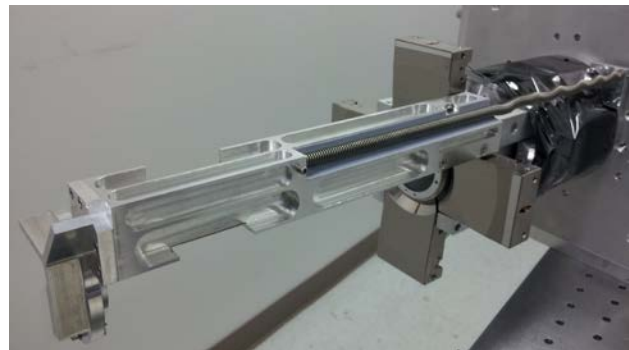**Figure 9: Deployable Secondary Stowed**

Figure 10. Deployable Secondary Deployed

Like the primary mirror mechanism, this mechanism is powered by a mechanical spring system that upon

release drives the metering structure from the stowed to deployed position. Damping is utilized to minimize the mechanism velocity and allow for a soft landing into the kinematic positioning mount. The kinematic positioning mount provides highly repeatable and accurate positioning.

During operation in space, the secondary mirror will deploy and passively self-align on the kinematic positioning mount. There are no additional compensating adjustments such as focus adjustment in order to simplify the system. This means that the secondary mirror needs to be very accurately positioned. Previous work[13] showed that the DPT image quality performance sensitivity to the secondary mirror is most sensitive to de-space relative to the primary mirror along the optical axis. For small errors the sensitivity is near linear and is less than 4 nm RMS system WFE for every micron of de-space error. Sensitivity to secondary mirror tilt is slightly less than 5 nm RMS system WFE for every minute of tip or tilt misalignment. Lastly sensitivity to secondary mirror de-center is 0.1 nm RMS system WFE for every micron of de-center misalignment.

Secondary Alignment Repeatability

Secondary mirror alignment repeatability testing was completed using the proof of principle hardware system. The bench top test setup is shown in Figure 11. An electronic autocollimator, with a measurement capability of 0.6 arc seconds, was used to measure tip/tilt repeatability errors from the flat back surface of the secondary. Precision micrometers with 0.5 µm resolution were used to measure de-space and de-center errors of the secondary metering structure. Direct contact of the precision micrometer with the secondary metering structure introduces a small measurement uncertainty to the test. This error and the associated subjectivity was minimized by sliding a thin piece of polished glass between the non-rotating micrometer head and the metering structure being measured. The micrometer would gently pinch the glass and was backed off until the glass fell by its own weight. The micrometer position at which the glass was released was recorded. Multiple tests of a single position using this measurement method shows measurement uncertainty of 1.4 µm.
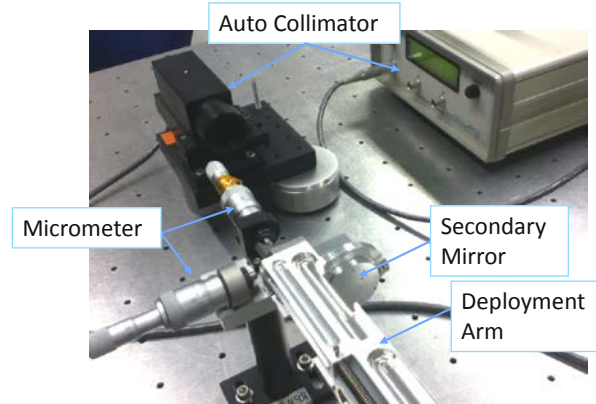

Figure 11: Bench Top Test Setup

Table 3 lists the deployable secondary alignment statistics for a total of 17 deployments. The test results show that the tip/tilt and de-center associated deployment repeatability errors are quite small and will have negligible effect on the DPT system imaging performance. De-space deployment repeatability errors are very small, however the system's high sensitivity to de-space means that these errors will have some impact to overall system imaging performance but it will be small. This high level of secondary mirror de-space deployment repeatability will not require the addition of an on-orbit active focus adjustment mechanism.

Table 3: Secondary Mirror Deployment Errors for 17 Deployments

Error Description	Measured 2σ	Resulting System RMS WFE [nm]	Measurement 1σ Uncertainty
Tip (Az)	8.2 arcsec	0.7 nm	0.6 arcsec
Tilt (El)	2.2 arcsec	0.2 nm	0.6 arcsec
De-Space	2.0 µm	7.1 nm	1.4 µm
De-Center	13.0 µm	1.3 nm	6.6 µm

System Image Quality Performance Prediction

The alignment repeatability statistics of the deployable primary and secondary mirrors is used in a system level image quality performance budget for fully deployed telescope operation. The analysis uses Cassegrain system level alignment sensitivities previously reported[13] and assumes the primary and secondary mirrors are manufactured with surface figures that support visible light imagery. Modern polishing methods should have no problem meeting a 15 nm RMS primary mirror surface error requirement. Since the secondary mirror is monolithic and much smaller it won't be difficult to polish it to better than half the figure error of the primary mirror. Table 4 presents the image quality tolerance budget with the eight major contributors to system level performance.

Table 4: System Errors and RMS Wavefront Error Contributions

Error Description	RMS Wavefront Error [nm]
Optical Design Residual	15.0
Primary Figure	30.0
Measured 2σ Primary Deployment	15.6
Secondary Figure	15.0
Measured 2σ Secondary De-Space	7.1
Measured 2σ Secondary Tip	0.7
Measured 2σ Secondary Tilt	0.2
Measured 2σ Secondary De-Center	1.3
RSS	40.6

Taking an RSS of all the error contributions gives an estimated system RMS wavefront error of 40.6 nm or an estimated peak-to-valley wavefront error of 163 nm[14]. Assuming the quarter-wave criterion for diffraction limited performance, this peak-to-valley wavefront error will yield diffraction limited imaging performance for wavelengths of 652 nm and above. This shows that image quality should be very good in the entire visible spectrum.

CONCEPTUAL CUBESAT HIGH RESOLUTION IMAGER

As a conceptual example, consider a high-resolution imaging CubeSat system utilizing the DPT. Consider also that the Cubesat is comprised of state-of-the-art, existing packable components.

Camera / Sensor Array

Camera sensors have been improving with new products commercially available. One of these relatively new innovations is the Live MOS® 17.3 X 13 mm sensor array with 4608 X 3456 array of 3.75 um pixels. This sensor is a CMOS (complementary metal oxide semiconductor) image sensor that boasts low noise high sensitivity similar to a full frame transfer (FFT) charge couple device (CCD) sensor with the low power requirements of a CMOS sensor[15]. Both Olympus and Panasonic offer commercially available cameras utilizing this sensor.

Optics

The optical payload is comprised of a 200 mm diameter F/7 Cassegrain telescope that can be stowed approximately within a 2-3U volume. Considering a NADIR pointing application at a 500 km altitude, the CubeSats relatively large aperture of 200 mm provides an optics ground spot size (OGS) of 1.5 m as calculated using Equation 1 where λ is the center wavelength, h is the height or satellite altitude, and D is the aperture diameter. The calculation assumes diffraction limited performance at 632.8 nm.

$$OGS = \frac{\lambda h}{D} \qquad (1)$$

The Cassegrain telescope form combined with a deploying secondary mirror allow for a relatively long 1.4 m focal length. Combining this focal length with the Live MOS® sensor results in an instantaneous field of view of 2.7 µrad and a ground sampling distance (GSD) of 1.3 m. The rectangular full field of view is 0.7° by 0.5° giving a ground coverage of 6.1 km by 4.6 km from a 500 km altitude.

Signal-to-Noise

An optical sensor signal-to-noise ratio (SNR) approaching 100 or higher will support most high-resolution extended source Earth imaging missions. SNR is calculated using Equation 2 and Equation 3 where Q_{Earth_Sol} is the sensor response to the solar illuminated Earth view and σ_{floor} is the pixel noise floor of the sensor chip.

$$SNR_{Earth\_Sol}\left(FN, t_{int}\right) = \frac{Q_{Earth\_Sol}\left(FN, t_{int}\right)}{\sqrt{\sigma^2_{floor} + Q_{Earth\_Sol}\left(FN, t_{int}\right)}} \qquad (2)$$

$$Q_{Earth\_Sol}\left(FN, t_{int}\right) = A_{Pix}\frac{\pi}{4FN^2}\tau_{tot}t_{int}\int_{400nm}^{900nm}\tau_\lambda dL_{p\_Earth\_Sol}d\lambda + I_{dark}t_{int} \qquad (3)$$

The sensor response Q_{Earth_Sol} is calculated in Equation 3 where A_{Pix} is the pixel area, FN is the F-number, τ_{tot} is the telescope transmission efficiency including aperture area factors, t_{int} is the sensor integration time, τ_λ is the filter transmittance, $dL_{p\_Earth\_Sol}$ is the solar illuminated Earth radiance at the telescope aperture, and I_{dark} is the sensor dark current.

Nominal day-time Earth viewing conditions are assumed for visible wavelengths extending to 900 nm in the near infrared. The sensor chip efficiency and noise parameters come from work done at Aptina Imaging concerning low noise high efficiency 3.75 µm global shutter CMOS pixel arrays[16]. Telescope parameters for the 200 mm DPT are used including the cross-shaped segmented primary mirror. For this analysis we assume that the small satellite cannot stabilize and track an object on Earth, which would allow for longer integration times. Because of this, the integration time is limited to be less than 0.18 ms by the relative motion of the satellite orbital velocity with respect to the targeted Earth scene smearing the imagery. For integration times longer than 0.18 ms it is anticipated that image smear will be excessive reducing the imagery resolution. Figure 12 shows SNR calculated with respect to integration time. For integration times of 0.18 ms a SNR close to 70 is predicted.
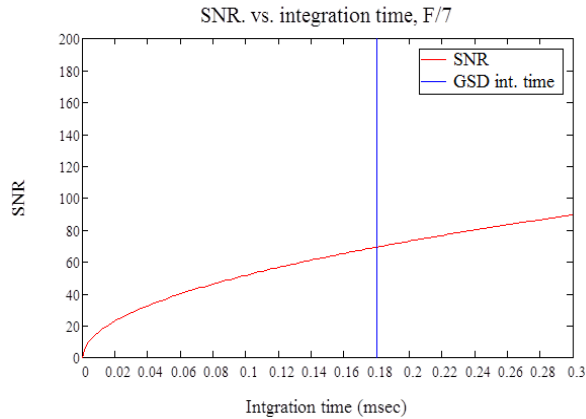
Figure 12: SNR plotted as a function of integration time with a vertical line representing the GSD limited maximum integration time

Image Data Handling

High-resolution imagery means that large amounts of data will need to be handled, stored, and downlinked. For the previously described sensor chip with a 12 bit format, 14.7 frames per second can be collected. Uncompressed raw file sizes are just under 24 MB. With typical compression, the resulting bitrate is close to 1.7 Gbps. Storage space of 850 GB is required for an hour of uncompressed data collection. Mission CONOPS and imagery compression techniques will need to be traded and selected to minimize data storage requirements and data downlink requirements. Data storage can be handled by state-of-the-art solid-state recorders that are available with data rate capabilities faster than 1 Gbps and storage capabilities higher than 1 terabyte[17]. The limiting factor in the data handling is the data transmission rates as missions are often able to store more than they can transmit. However, Syrlinks[18] has developed a miniaturized X-band transmitter that, with a dedicated operating transmission mode, can transmit down to a 5 m ground station up to 13.3 GB per orbital pass.

Packaging, Mass, and Power

For this conceptual high-resolution imaging CubeSat we have discussed components that have been designed for CubeSat implementation including state-of-the-art high performance DPT, sensor, solid-state recorder, and X-band transmitter. Packaging within the limited CubeSat volume, mass and power requirements, and system budgets have not been addressed in detail. We realize that trades will need to be made and customizations may be required to provide packaging flexibility. For instance, packaging the camera may require a flex harness connecting the sensor chip assembly to the camera electronics. This can be very useful for packaging the camera in constraining volumes.

Other components including the bus, solar arrays, thermal management hardware, telescope baffling, attitude determination and control systems have not been addressed. The authors do not see these unaddressed components as areas of high concern that may negate the feasibility of a high-resolution CubeSat system.

The development of the DPT, high performance CMOS cameras, solid-state recorders, and X-band transmitters as well as other advancing technologies together show that obtaining high quality, high precision imagery from a CubeSat class space vehicle is realizable and should be considered in future science mission planning.

CONCLUSION

The development of deployable optics is an important stepping stone towards the realization of near meter class ground spatial resolution captured from a CubeSat class satellite. Current Earth observation satellites have aperture diameters greater than 300 mm in order to meet mission requirements. Over the past three years, the Space Dynamics Laboratory has been researching and developing deployable segmented mirrors and metering structures designed for CubeSats. Alignment repeatability of a deployable primary and secondary mirror was measured and shown to be capable of supporting visible light imagery in a long focal length Cassegrain optical configuration. A conceptual CubeSat imager that incorporates a 200 mm aperture diameter deployable petal telescope and state-of-the-art commercial components is able to produce 1.5 m ground spatial resolution with a signal-to-noise ratio close to 70. Commercial transmitters and solid state recorders are available that can store and transfer the large amounts of data produced by this high-resolution imaging system. Many technology developments have come together to make the feasibility of high-resolution CubeSat based imaging much closer to a reality.

Acknowledgments

References

1. Domber, J., Hinkle, J., Peterson, L., Warren, P., "Dimensional Repeatability of an Elastically Folded Composite Hinge for Deployed Spacecraft Optics," Journal of Spacecraft and Rockets, Vol. 39, No. 5, Sept.-Oct. 2002.

2. Lillie, C. "Large Deployable Telescopes for Future Space Observatories," Northrop Grumman Corporation, One Space Park, Redondo Beach, CA 90278.

3. Lane, S., Lacy, S., Babuska, V., Hanes, S., Schrader, K., Fuentes, R., "Active Vibration Control of a Deployable Optical Telescope," Journal of Spacecraft and Rockets, Vol. 45, No. 3, May-June 2008.

4. Andersen, G., Asmolova, O., Dearborn, M., McHarg, M., "FalconSAT-7: A Membrane Photon Sieve Cubesat Solar Telescope," Space Telescopes and Instrumentation 2012: Optical, Infrared, and Millimeter Wave.

5. Agasid, E., Ennico-Smith, K., Rademacher, A., "Collapsible Space Telescope (CST) for Nanosatellite Imaging and Observation," 2013 AIAA/USU Conference on Small Satellites, Logan, UT, Aug 2013.

6. Greenbaum, A., Knapp, M., Schaalman, G., Henderson, T., Seager, S., "Low-mass High-performance Deployable Optical Baffle for Cubesats,"

7. Stiles, L., Garrett, J., Murphey, T., Dumm, H., Banik, J., "Development of Deployable Aperture Concepts for CubeSats," 51st AIAA/ASME/ASCE/AHS/ASC Structures, Structural Dynamics, and Materials Conference, 2010.

8. Cawthorne, A., Purll, D., Eves, S., "Very high resolution imaging using small satellites," AIAA 6th Responsive Space Conference, 2008.

9. "DubaiSat-2", https://directory.eoportal.org/web/eoportal/satellite-missions/d/dubaisat-2, 24 May, 2014.

10. Kim, E., Choi, Y., Kang, M., Jeong, S., "Development of Earth Observation Sensors for Small Satellites in SaTReC Initiative," Proceedings of the 5th IAA Symposium on Small Satellites for Earth Observation, Berlin, Germany, April, 2005.

11. Butler, D., "Many eyes on Earth," Nature News and Comment, 505(7482), 8 January 2014.

12. "Plant Labs' Remote Sensing Satellite System," Cubesat Developers Workshop, Logan, Utah, 2013.

13. Champagne, J.A., Crowther, B.G., and Newswander, T.T., "Deployable Mirror for Enhanced Imagery Suitable for Small Satellite Applications", 2013 AIAA/USU Conference on Small Satellites, Logan, UT, Aug 2013.

14. Smith, W.J., Modern Optical Engineering, The Design of Optical Systems, page 374, Fourth Edition, McGraw Hill, New York, 2008.

15. "Micro Four Thirds Products – Cameras," http://www.four-thirds.org/en/microft/body.html, 25 June, 2014.

16. Sergey Velichko[1], Gennadiy Agranov[2], Jaroslav Hynecek[2], Scott Johnson[1], Hirofumi Komori[2], Jenny Bai[2], Igor Karasev[2], Rick Mauritzson[1], Xianmin Yi[2], Victor Lenchenkov[2], Sarah Zhao[2], Hyuntae Kim[1],[1]Aptina, Meridian, ID, USA, [2]Aptina, San Jose, CA, USA, "Low Noise High Efficiency 3.75 µm and 2.8 µm Global Shutter CMOS Pixel Arrays"

17. David Biggs, John Conley, Andres Dono Perez, Nicolas Faber, Anthony Genova, Andrew Gonzales, Alessandro Grasso, James Harpur, Steven Hu, Luke Idziak, Sarah Jolitz, Jonas Jonsson, John Love, Yosuke Nakamura, Andrew Nuttall, Robin Reil, Vibha Srivastava, Travis Swenson, and Sasha Weston NASA/TP–2014–216648 Small Spacecraft Technology State of the Art; *Mission Design Division Staff Ames Research Center, Moffett Field, California* Feb 2014;

18. "Very High Data Rate Transmitter in X-Band for CubeSat and NanoSatellite Platforms", http://www.syrlinks.com/en/products/cubesat-and-nanosatellite-platforms.html, 25 June, 2014.